

The Mechanics of *Arabidopsis* Seed Germination

Problem presented by

Tara Holman, Darren Wells, Michael Wilson, Susana Ubeda-Tomas,
Andrew French and Michael Holdsworth
School of Biosciences, University of Nottingham, UK

January 24, 2008

Report prepared by

A.M. Middleton, R.J. Dyson, L.R. Band, S. Grandison, D.M. Wells, T.J. Holman, J. Twycross,
O. E. Jensen

1 Introduction

Arabidopsis thaliana is a higher plant, propagated through seed production. One *Arabidopsis* plant can produce many hundreds of thousands of seed through the course of one flowering cycle.

Arabidopsis seeds are extremely small — a dry seed weighs around 15 ng and is approximately spherical with a diameter of 200 μm . The seed is almost entirely composed of the embryo, which is filled with lipid and protein reserves to fuel germination and establishment prior to photosynthesis. Surrounding the embryo is a single-cell layer of endosperm (also of zygotic origin), covered by the dead, maternally derived testa (seed coat) (figure 1). These two tissues envelop the radicle, a region of the seed which forms the root of the plant [8].

Germination is defined as the protrusion of the radicle through both layers (endosperm and testa) [2]. As the radicle elongates, the testa ruptures. This is followed by rupture of the endosperm at the micropylar end of the seed. *Arabidopsis* seeds exhibit a two-step germination process, with sequential testa and endosperm rupture (figure 2) [3].

The testa is metabolically inactive in the mature seed. The function of the endosperm is not wholly understood, although abscisic acid (ABA), a phytohormone known to negatively control germination, has been shown to be synthesised within this tissue [4].

The transition from a dry seed to a seedling is triphasic according to uptake of water. Phase I is imbibition — the physical process of water uptake into the dry seed. During imbibition, the seed swells to an ellipsoid with a length of around 350 μm and diameter of around 250 μm . During phase II there is a plateau in water uptake. A further increase in water uptake at phase III signals the end of germination and the start of post-germinative growth. Phase III is concurrent with the elongation of the embryonic axis and protrusion of the radicle through the seed coat [2]. Although it is widely accepted that radicle extension occurs via cell elongation, there are conflicting reports as to whether cell division is also required for germination [1, 7].

The endosperm provides both chemical and mechanical resistance to germination. For the completion of germination, the cell walls of the endosperm must be modified to allow the radicle to protrude. In tomato, weakening of the endosperm is required for germination to occur [?]. There is evidence that genes encoding cell-wall remodelling enzymes are expressed in both the embryo and endosperm [10]. The expression levels of these genes are controlled by the phytohormones ABA and gibberellins (GA). ABA and GA have an antagonistic effect on germination - GA promotes germination whilst ABA represses it. ABA is able to prevent germination by inhibiting endosperm rupture, although testa rupture still occurs [9].

Arabidopsis seeds are too small (500 μm) to allow mechanical testing, but experiments using the related species *Lepidium* have shown that the force required to puncture the endosperm varies from 40 mN to 20 mN over 18 h (during which the percentage of germinated seeds in the test population rose from 0 to 72%). This force is presumably provided by the growing radicle.

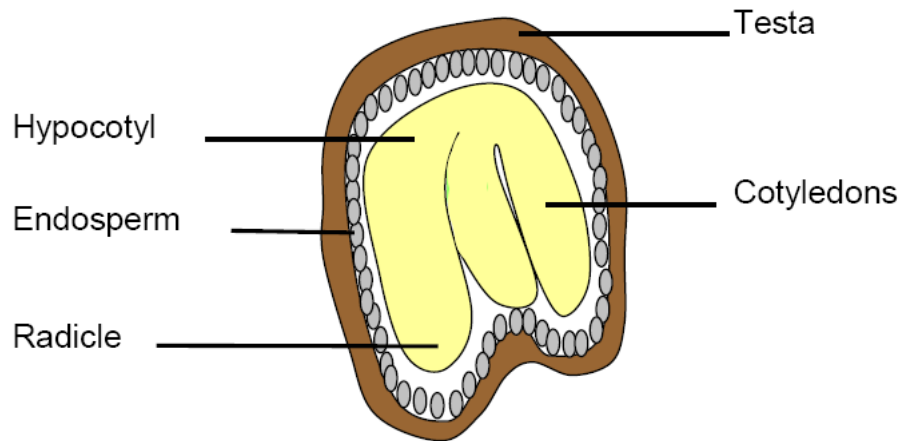


Figure 1: The structure of an *Arabidopsis* seed. A diagrammatic representation of a mature *Arabidopsis* seed, consisting of a diploid embryo surrounded by a single layer of triploid endosperm cells. The endosperm is covered by the testa [8]. (Diagram is not to scale.)

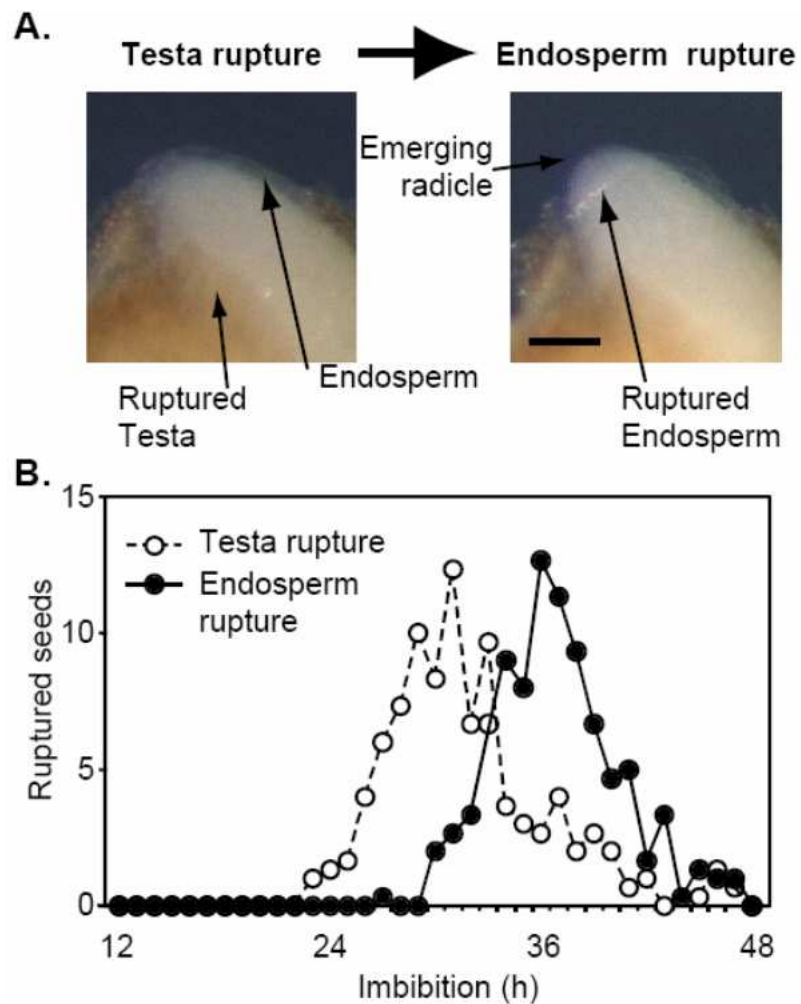


Figure 2: Endosperm and testa rupture are distinct events. Testa rupture occurs after around 35 hours of imbibition, approximately 5 hours prior to endosperm rupture [3].

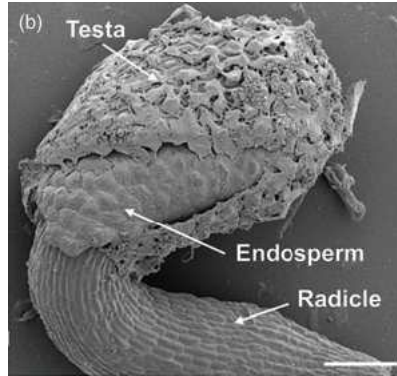


Figure 3: Micrograph of germinated *Arabidopsis* seedling. Note the cells of the endosperm, which remain alive after germination, are relatively intact (scale bar = 100 μm , image from [5]).

Models of plant cell growth have been developed, the most well-known being that of Lockhart [6] which describes growth as a mechano-hydraulic process:

$$\frac{1}{V} \frac{dV}{dt} = \frac{\phi L}{\phi + L} (\Delta\Psi + P - Y), \quad (1)$$

where V is the cell volume, L is the water conductance coefficient, P is the turgor pressure, ϕ is the extensibility, Y is the yield threshold, and $\Delta\Psi$ is the water potential difference.

Anisotropic (directional) growth is believed to result from cell-wall remodelling (corresponding to an alteration of ϕ in the model (1)). It is interesting to note that endosperm weakening also probably involves alteration in wall properties, perhaps indicating a common mechanism that drives radicle growth, whilst reducing endosperm resistance. Electron micrographs of germinated seedlings show the structure of the endosperm to be relatively intact after protrusion of the radicle, suggesting that rupture occurs between individual cells rather than by breakage of cell walls (figure 3).

Whilst much effort has been placed on the genetic networks involved in this process, a mathematical approach for furthering the understanding of the physical/mechanical properties of germination has not yet been described. Many of the required parameters, such as the kinetics of water uptake, are available from the literature [11, 12].

Modelling the mechanics of germination will aid biological researchers in their understanding of the system, and may help to develop novel strategies for producing seeds with uniform germination patterns.

1.1 Modelling strategy

The key process in germination is the rupture of the endosperm. Therefore, in this report, we ignore the testa rupture, and model only the proceeding dynamics. We develop a range of models to investigate the growth of the radicle (which is inhibited by the surrounding endosperm) and the weakening, stretching and rupture of the micropylar region of endosperm. We consider separate models for the radicle and the endosperm; although coupling these models would provide further understanding it is beyond the scope of this report.

In §2, we model the radicle elongation, representing the endosperm as a force on the ends of the radicle. We show the length of the radicle gradually increases until it reaches a critical length, at which the endosperm ruptures (*i.e.* the force on the ends of the radicle drops to zero), and the radicle's length rapidly increases.

We investigate the stretching and rupture of the endosperm in §3, assuming that the radicle provides a force normal to the endosperm. As the appropriate choice for the material properties of the endosperm is unclear, we consider several models. In §3.2–3, we assume the endosperm is elastic. We first consider a simple elastic spring model and use experimental data to prescribe

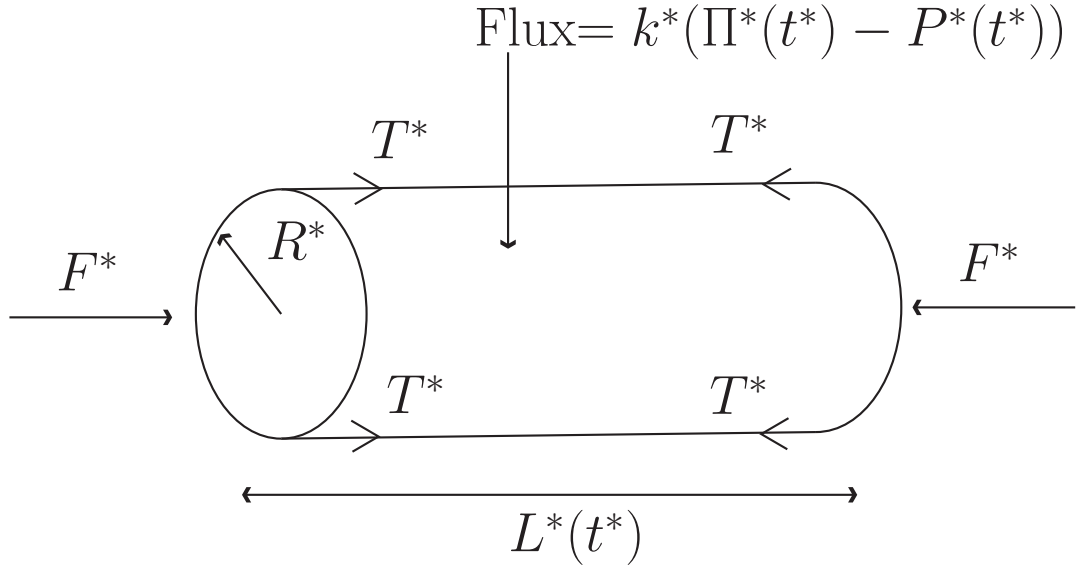


Figure 4: Diagram of the radicle model (2)-(6).

the weakening of the endosperm (§3.2). We then show how this spring model could be developed into a more complex computational model which consists of a sheet of rigid cells joined by elastic springs (§3.3). In §3.4–5, we assume the endosperm is viscous. In §3.4, we develop a ‘Lockhart-style’ model, considering the stretching of the individual cells in the endosperm. We then consider a tissue-scale model in §3.5, modelling the endosperm as a thin viscous sheet. In §4, we summarise our progress and discuss potential future work.

2 Radicle elongation

2.1 Model

In this section, we develop a ‘Lockhart-style’ model of radicle elongation. We model the radicle as a cylinder of fluid and investigate how the length of the radicle changes in response to osmotic potential. The action of the endosperm on the radicle is represented by a force F^* , opposing radicle growth. We assume that the endosperm ruptures once the radicle reaches a critical length.

Details of the model are summarised in figure 4. We model the radicle as a cylinder of length $L^*(t^*)$ and radius R^* (which we assume to be constant). The radicle has osmotic potential $\Pi^*(t^*)$, which the radicle regulates in order to keep the turgor pressure, $P^*(t^*)$, approximately constant. We assume that, without loss of generality, the fluid surrounding the radicle is at zero hydrostatic pressure and osmotic potential. The turgor pressure acts on the ends of the radicle, and induces a tension, $T^*(t^*)$, in the radicle walls. We assume that if this tension is greater than a prescribed yield stress, Y^* , the radicle will lengthen. The extensibility of the radicle walls is denoted by μ^* , and the permeability of the radicle walls is denoted by k^* .

We use this model to investigate the relationships between the four variables: the length of the radicle, $L^*(t^*)$, the tension in the radicle walls, $T^*(t^*)$, the turgor pressure, $P^*(t^*)$, and the osmotic potential, $\Pi^*(t^*)$. In particular, this model enables us to see how the variables change when the radicle suddenly breaks through the endosperm and F^* drops to zero.

2.2 Governing equations

The flux into the radicle (across the sides of the cylinder) changes the radicle's volume. Thus, by conservation of mass, we obtain

$$\frac{d(\pi R^{*2} L^*)}{dt^*} = 2\pi R^* L^* k^* (\Pi^* - P^*), \quad (2)$$

which reduces to

$$\frac{1}{L^*} \frac{dL^*}{dt} = \frac{2k^*}{R^*} (\Pi^* - P^*). \quad (3)$$

Balancing the forces on the ends of the radicle, we find the turgor pressure, $P^*(t^*)$, and tension in the radicle walls, $T^*(t^*)$, balances the force exerted on the radicle by the endosperm, F^* . Therefore, by the conservation of momentum, we find that

$$F^* = \pi P^* R^{*2} - 2\pi R^* T^*. \quad (4)$$

Once the tension, $T^*(t^*)$, is above the prescribed yield stress, Y^* , the radial stretches according to

$$T^* - Y^* = \mu^* \frac{dL^*}{dt^*}. \quad (5)$$

where μ^* is the extensibility of radicle walls. The osmotic potential is regulated to maintain the pressure inside the radicle, P^* , equal to the optimal turgor pressure, \hat{P}^* . Hence, we write

$$\frac{d\Pi^*}{dt^*} = -A^* (P^* - \hat{P}^*), \quad (6)$$

where A^* is a constant with dimensions s^{-1} .

2.2.1 Nondimensionalisation

We base the length of the radicle on its initial length, L_0^* . The characteristic timescale is the rate of water flux into the radicle, namely $R^*/(k^*\hat{P}^*)$, and the characteristic pressure is the optimal turgor pressure \hat{P}^* . We make the following rescalings

$$L^* = L_0^* L, \quad t^* = \frac{R^*}{k^* \hat{P}^*} t, \quad \Pi^* = \hat{P}^* \Pi, \quad P^* = \hat{P}^* P, \quad (7)$$

and we obtain the dimensionless regulation rate, extensibility and yield stress

$$\alpha = \frac{k^* \hat{P}^*}{A^* R^*}, \quad M = \frac{\mu^* L_0^* k^*}{R^{*2}}, \quad \mathcal{Z} = \frac{F^*}{2\pi R^{*2} P^*} + \frac{Y^*}{\hat{P}^* R^*}. \quad (8)$$

Note that the action of the endosperm, F^* , merely modifies the effective yield stress of the walls. It then follows from (2)-(6) that the dimensionless governing equations are

$$M \frac{dL}{dt} = \frac{P}{2} - \mathcal{Z}, \quad (9a)$$

$$\frac{1}{L} \frac{dL}{dt} = 2(\Pi - P), \quad (9b)$$

$$\alpha \frac{d\Pi}{dt} = 1 - P. \quad (9c)$$

2.2.2 Parameter regimes

Typical parameter values are

$$\begin{aligned} k^* &= 0.1 \mu\text{ms}^{-1} \text{MPa}^{-1}, & \hat{P}^* &= 0.05 \text{MPa}, & A &= 0.1 \text{s}^{-1}, \\ \mu^* &= 200 \text{MPa s}, & R^* &= 100 \mu\text{m}, & L_0^* &= 100 \mu\text{m}. \end{aligned} \quad (10)$$

The turgor pressure (\hat{P}^*) was obtained from [13]. The remaining parameter values were estimated from video of a germinating seed. The footage was provided by S. Ubeda-Tomas and A. French. It follows from (8) that $\alpha = 6 \times 10^{-3} \ll 1$, $M = 0.2$.

2.3 Model solutions

We proceed by considering solutions to (9) for $0 < \alpha \ll 1$. It follows from (9c) that for this special case $P \sim 1$, *i.e.* the pressure rapidly adjusts to attain full turgor. From (9a) and (9b) we learn that

$$\frac{dL}{dt} = \frac{1 - 2\mathcal{Z}}{2M}, \quad (11a)$$

$$\Pi - 1 = \frac{1 - 2\mathcal{Z}}{4ML}, \quad (11b)$$

so osmotic potential (Π) decreases as the length of the radicle (L) increases. We require that the tension T^* is above yield stress Y^* and in dimensionless terms this condition corresponds to $1 > 2\mathcal{Z}$.

To study the radicle breaking through the endosperm we choose

$$F = k(L - L_c), \quad (12)$$

(so that the endosperm tissue is elastic with modulus k and natural length L_c) until $L = L_r$ when the endosperm ruptures. By (8), \mathcal{Z} becomes

$$\mathcal{Z} = \begin{cases} Y + \beta(L - L_c), & \text{for } L < L_r \\ Y, & \text{for } L > L_r \end{cases} \quad (13)$$

where, in terms of dimensional parameters,

$$Y = \frac{Y^*}{\hat{P}^* R^*}, \quad \beta = \frac{k^*}{2\pi R^2 \hat{P}^*}. \quad (14)$$

Therefore, \mathcal{Z} drops when the endosperm ruptures. Substituting (13) into (11a) the equation governing radicle elongation becomes

$$2M \frac{dL}{dt} = 1 - 2(Y + \beta(L - L_c)), \quad (15)$$

for $L < L_r$.

Numerical solutions to (11) are shown in figure 5. It follows from (11a) that provided $1 > 2\mathcal{Z}$, L increases monotonically and so the radicle grows steadily. The osmotic potential (Π) is slaved to length (L) with its dependence given in (11b). From this we see that as $L \rightarrow \infty$, $\Pi \rightarrow 1$. By (13), as L passes through L_r , \mathcal{Z} drops to its constant value, Y , causing Π to increase so as to maintain turgor pressure *i.e.* the osmotic potential increases to account for the rupture of the endosperm. This in turn causes the rate of radicle growth (\dot{L}) to increase.

3 Endosperm model

3.1 Introduction

In this section we model the stretching and rupture of the endosperm. As the radicle elongates it applies a force to the micropylar region of the endosperm, and in addition, the micropylar region is weakened by cell-wall remodelling enzymes [9]. These two key processes cause the cells in the endosperm to stretch, and eventually some of the walls between adjacent cells rupture, allowing the radicle to emerge.

The deformation of the endosperm depends crucially on the material properties of the tissue; however, the appropriate choice of constitutive model remains unclear. For comparison, in sections 3.2 and 3.3, we consider an elastic model of the endosperm, whereas in sections 3.4 and 3.5, we model it as a viscous fluid.

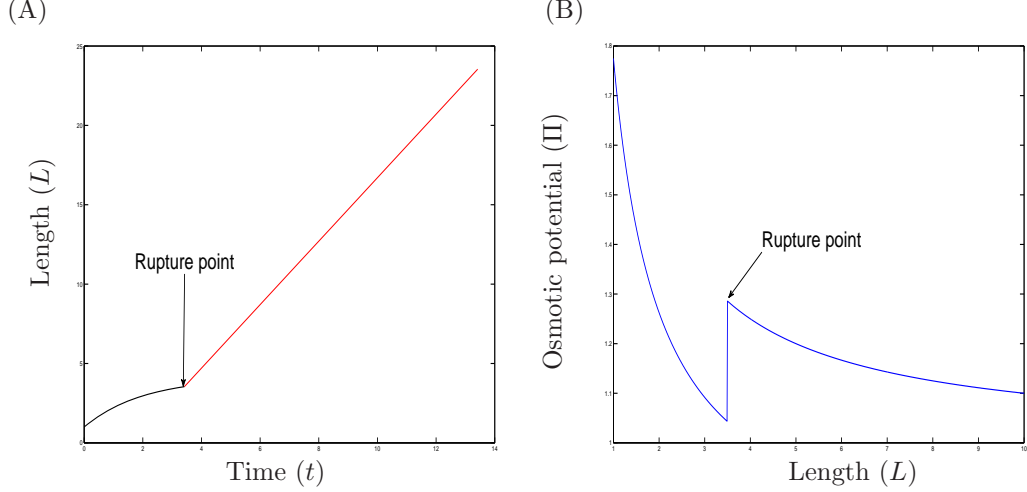


Figure 5: Numerical solutions to (11a) and (11b) for \mathcal{Z} in (13). (A) Plot of radicle length against time. When the endosperm ruptures, the rate of radicle growth increases. (B) Plot of osmotic potential against length. The osmotic potential increases when the endosperm ruptures to maintain turgor pressure. The following parameter choices were made: $M = 0.2$, $L_c = 0.1$, $Y = 0.1$ and $\beta = 0.1$.

3.2 Analytical version of the endosperm spring model

In this section we model the micropylar region of the endosperm as a one-dimensional elastic material, as illustrated in figure 6. We assume that the ends of the endosperm are fixed, a distance $2l$ apart. The elongation of the radicle is represented as a constant point force, F , applied to the midpoint of the endosperm. This force causes the midpoint of the endosperm to be displaced a distance x , and so each half of the endosperm is stretched from length l to length $\sqrt{l^2 + x^2}$. Thus, by Hooke's law, the tension T in the endosperm walls is

$$T = k(t)(\sqrt{l^2 + x^2} - l), \quad (16)$$

where $k(t)$ is the time-dependent elastic modulus. We model the weakening of the endosperm by choosing $k(t)$ to be a monotonically decreasing function in t , and for simplicity, we assume a linear relationship:

$$k(t) = A - Bt, \quad (17)$$

where A and B are constants to be determined. The tension in the endosperm, (16), balances with the prescribed force F being generated by the radicle; applying a force balance, we find that

$$\begin{aligned} F &= -2 \cos(\theta)T, \\ &= 2k(t)(\sqrt{l^2 + x^2} - l) \frac{x}{\sqrt{l^2 + x^2}}, \\ &= 2k(t)x \left(1 - \frac{l}{\sqrt{l^2 + x^2}} \right). \end{aligned} \quad (18)$$

By fitting (18) to the available experimental data [9]

$$\begin{aligned} t = 4h, \quad x = 0.25 \times 10^{-3}m, \quad F = 19mN, \quad l = 0.25 \times 10^{-3}m, \\ t = 14h, \quad x = 0.75 \times 10^{-3}m, \quad F = 19mN, \quad l = 0.25 \times 10^{-3}m, \end{aligned}$$

we obtain

$$A = 170000, \quad B = 3.1. \quad (19)$$

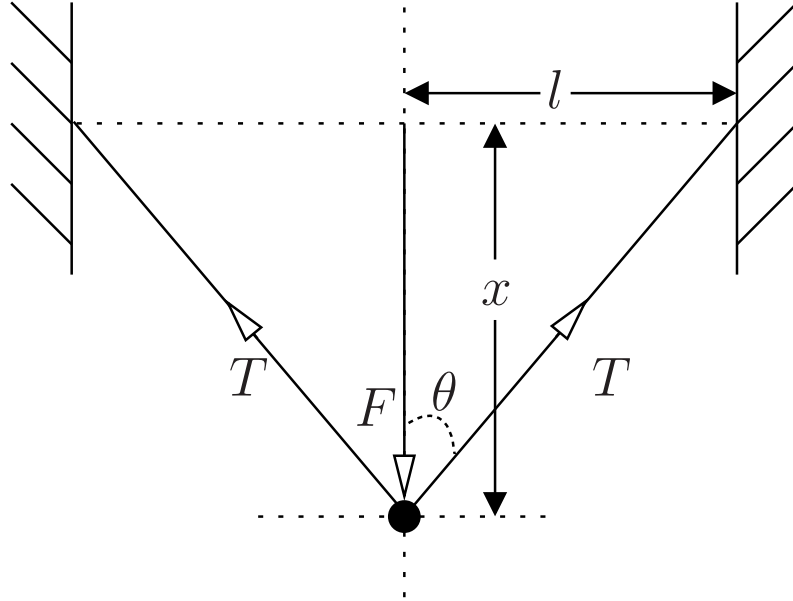


Figure 6: Diagrammatic representation of the endosperm spring model (16)-(18).

Figure 3.2 shows how the displacement x increases as the endosperm weakens, using the parameter values (19).

3.3 Mechanical ‘spring’ simulation

3.3.1 Introduction

In this section we model the endosperm as a sheet of elastic material.

3.3.2 Model details

We created a mechanical simulation of the endosperm surface, the pressure exerted by the radicle and the mechanical failure of the endosperm using an explicit Euler time-marching scheme. Code was developed to simulate the expansion and subsequent failure as a series interconnecting springs where the elastic modulus of the springs in the simulation could be altered individually.

We incorporate cell-wall thickness and bending stress into our model by creating a spring network consisting of several layers. A regularly spaced grid of nodes is created (these are the junction points where springs are connected) of dimension $N \times M \times P$. Typical dimensions chosen for the results shown later is a face of size $N = M = 16$ and a thickness of $P = 3$. During a simulation there are two distinct forces acting upon each node. First there is the net resultant force upon the node caused by the extension and compression of the springs, second there is an internal hydrostatic pressure that acts normal to the spring surface. For further details of the simulation see Grandison *et al*, 2007 (submitted to Journal of Theoretical Biology).

To simulate mechanical breakage the stress in each spring element is measured after each simulation frame is drawn. Springs whose stress have exceed a prescribed critical value are removed before the next frame is calculated in order to simulate breakage.

Figure 8 shows a number of frames from a typical simulation with the detail of the spring network shown, making the relative amount of stretching in each part of the network clear. The first spring breakage occurs shortly after frame 80, however the structure remains relatively stable for some time longer before undergoing a complete mechanical failure and breaking apart shortly before frame 140.

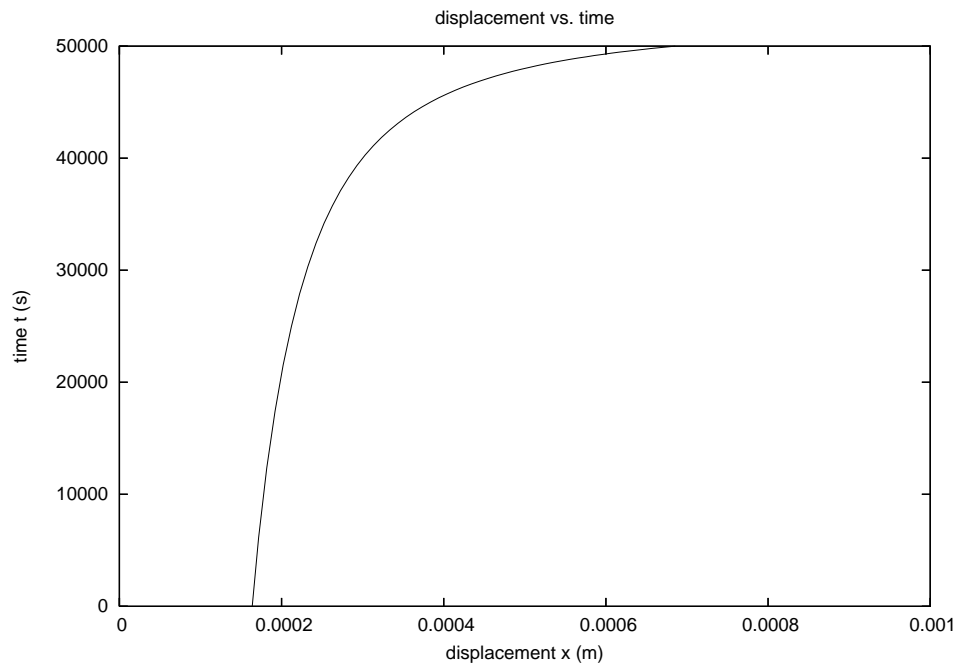


Figure 7: As the endosperm weakens, the displacement of the endosperm, x , increases.

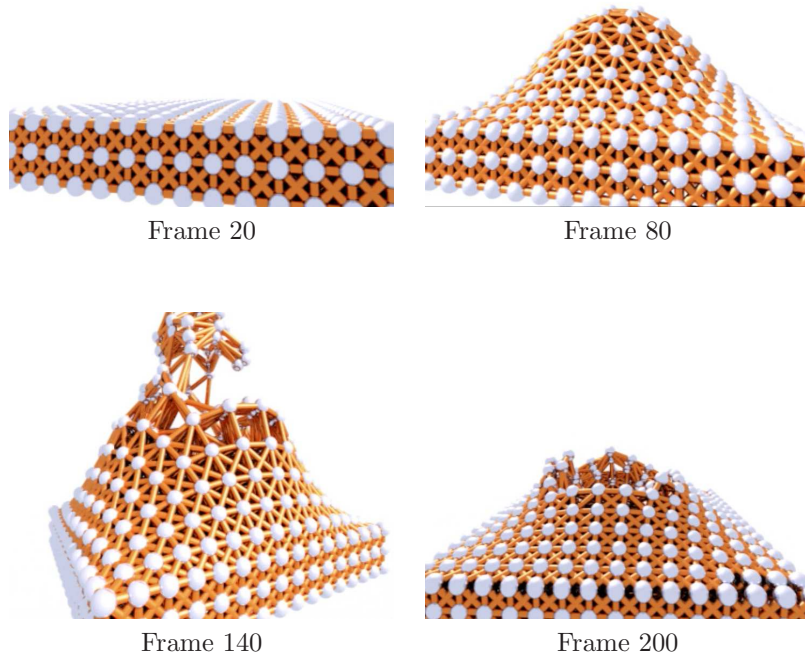


Figure 8: Four typical frames takes from a simulation of endosperm breakage.

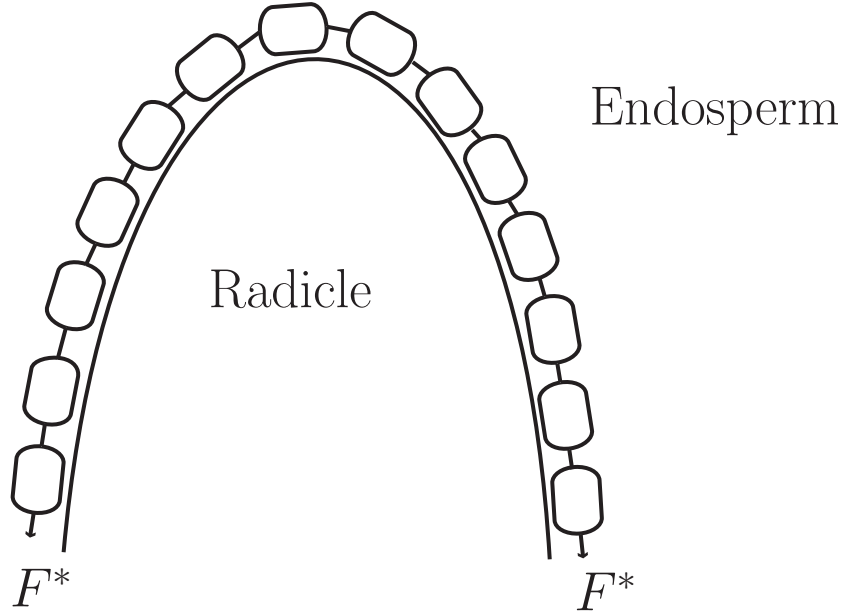


Figure 9: Diagrammatic representation of the Lockhart endosperm model (21)-(24).

3.4 Cell-scale viscous endosperm model

We now develop a ‘Lockhart-style’ model of the endosperm to investigate how the cells in the endosperm stretch. We model the endosperm as a string of N cells, as illustrated in figure 3.4. As the radicle elongates, it exerts a pressure on cell i of $P_{R_i}^*(t^*)$ at time t^* . We assume this results in a constant force along the line of cells, which we denote by F^* . The shape of the radicle determines the shape of the endosperm, and therefore prescribes the angle of cell i to the horizontal, which we denote by $\theta_i(t^*)$.

As the endosperm stretches, the total length of the micropylar region, $\lambda^*(t^*)$, will increase, and each cell in the micropylar region will lengthen. We take each cell i to have length $l_i^*(t^*)$ at time t^* , and assume that all the cells have equal cross-sectional area A^* , which is constant in time. We denote the position of each cell along the line of cells by $s_i^*(t^*)$ (so that $s_{i+1}^*(t^*) - s_i^*(t^*) = l_i^*(t^*)$). It follows that as the endosperm stretches, the velocity of a cell around the endosperm, $u_i^*(t^*)$, is given by

$$u_i^* = \frac{ds_i^*}{dt^*}. \quad (20)$$

We denote the osmotic potential of each cell by $\Pi_i^*(t^*)$. We assume that, as shown in §2, the regulation of the turgor pressure is rapid, so that each cell remains fully turgid at constant pressure P^* (where we have dropped the hat used in §2 to denote the optimal pressure). Without loss of generality, we assume the hydrostatic and osmotic pressures of the fluid surrounding the endosperm are zero. The internal pressure within the cells generates a tension in the wall of each cell $T_i^*(t^*)$. If the tension in the cell wall is greater than a prescribed yield stress, Y^* , the cell wall will lengthen. The permeability of the cell walls is denoted by k^* . Cell-wall remodelling enzymes cause the cell wall to weaken [9], and as suggested by Lockhart, we assume that the cell-wall weakening modifies the extensibility of the cell wall. Thus, to phenomenologically capture the cell-wall weakening, we prescribe a time-dependent extensibility, $\mu_i^*(t^*)$.

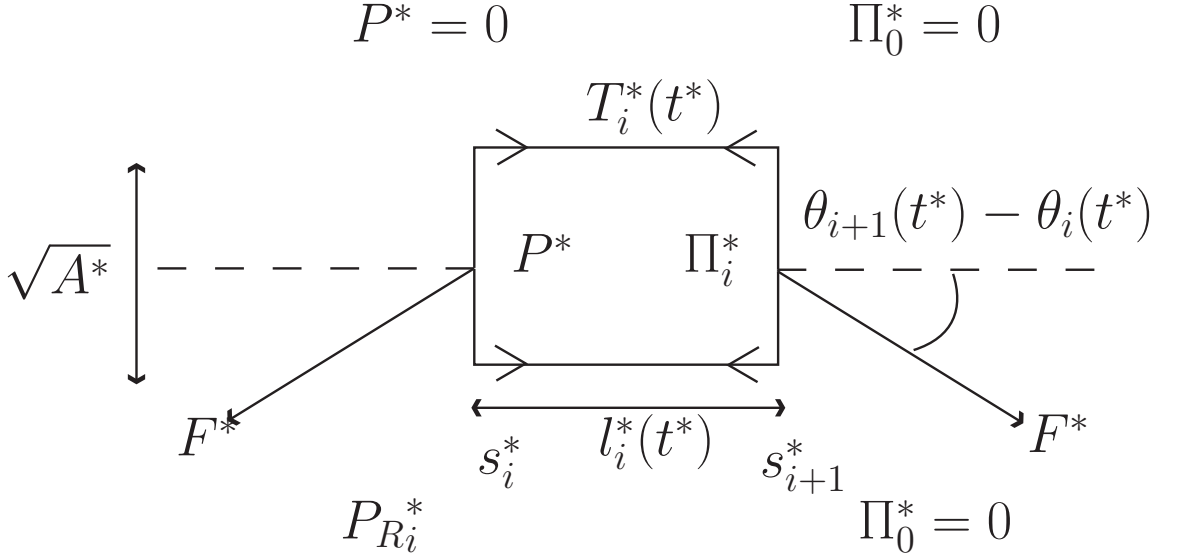


Figure 10: Diagram of the viscous endosperm model (21)-(24) for a single cell .

3.4.1 Governing equations

The flux of water into each cell changes the cell's volume. Recalling that the cross-sectional area of each cell, A^* , is assumed to be held constant, conservation of mass requires

$$A^* \frac{dl_i^*}{dt^*} = k^*(\Pi_i^* - P^*)l_i^* + k^*(\Pi^* - P^* + P_{Ri}^*)l_i^* + k^*(\Pi_i^* - \Pi_{i-1}^*)A^* + k^*(\Pi_i^* - \Pi_{i+1}^*)A^*, \quad (21)$$

where k^* is the cell-wall permeability. The force that the radicle exerts on the endosperm, P_{Ri}^* , induces an additional force F^* along the endosperm (see figure 3.4). Normal to each cell, the force F^* balances the pressure exerted on the endosperm by the radicle, whereas the component of F^* acting tangentially to each cell balances the tension induced by the turgor pressure in the cell walls, $T_i^*(t^*)$. Thus, balancing the force on each cell in the normal and tangential directions, we obtain

$$P_{Ri}^* l_i^* = F^*(\theta_{i+1} - \theta_{i-1}), \quad F^* \cos(\theta_{i+1} - \theta_{i-1}) = 2T_i^* - P^* A^*, \quad (22)$$

respectively. If the tension in the cell walls, $T_i^*(t^*)$, is greater than the yield stress, Y^* , the tension causes the cell walls to stretch. For $T_i^*(t^*) > Y^*$, the extension of cell i is governed by

$$T_i^* - Y^* = \mu_i^* \frac{dl_i^*}{dt^*}, \quad (23)$$

where $\mu_i^*(t^*)$ is the prescribed time-dependent cell-wall extensibility.

To summarise, the five unknown variables are the length of each cell, $l_i^*(t^*)$, the velocity of each cell round the endosperm, $u_i^*(t^*)$, the tension in the cell walls, $T_i^*(t^*)$, the osmotic potential of each cell, $\Pi_i^*(t^*)$, and the force induced in the endosperm, F^* , due to the pressure of the radicle. These variables are governed by the five equations (20-23). We assume that the initial cell length is $l_i^*(0) = \sqrt{A^*}$. We let the left-hand-side of the micropylar region of the endosperm be stationary, and the right-hand-side of the micropylar region move as the endosperm stretches. Therefore our boundary conditions are

$$u_1^*(t^*) = 0, \quad u_{N+1}^*(t^*) = \frac{d\lambda^*}{dt^*}. \quad (24)$$

3.4.2 Nondimensionalisation

We now nondimensionalise the governing equations (20)-(23) by adopting the following scalings:

$$\begin{aligned} (F^*, P_{Ri}^*, \Pi_i^*) &= P^*(F, P_{Ri}, \Pi_i), & (s_i^*, l_i^*, \lambda^*) &= \sqrt{A^*}(s_i, l_i, \lambda), & T_i^* &= P^*\sqrt{A^*}T_i, \\ t^* &= \frac{\sqrt{A^*}}{P^*k^*}t, & \mu_i^* &= \frac{\sqrt{A^*}}{k^*}\mu_i, & u_i^* &= P^*k^*u_i. \end{aligned} \quad (25)$$

We obtain the dimensionless parameter

$$Y = \frac{Y^*}{P^*\sqrt{A^*}}, \quad (26)$$

which represents the dimensionless yield stress.

Upon applying these scalings, (25), to (20)-(23), we obtain the following dimensionless governing equations. Conservation of mass requires

$$\frac{dl_i}{dt} = 2(\Pi_i - 1)l_i + P_{Ri}l_i - \Pi_{i+1} + 2\Pi_i - \Pi_{i-1}, \quad (27)$$

and conservation of momentum is given by

$$T_i - Y = \mu_i \frac{dl_i}{dt}, \quad (28a)$$

$$P_{Ri}l_i = F(\theta_{i+1} - \theta_{i-1}), \quad (28b)$$

$$F \cos(\theta_{i+1} - \theta_{i-1}) = 2T_i - 1. \quad (28c)$$

The geometry is determined by

$$l_i = s_{i+1} - s_i \quad u_i = \frac{ds_i}{dt},$$

which reduces to

$$\frac{dl_i}{dt} = u_{i+1} - u_i. \quad (29)$$

The boundary conditions, (24), become

$$u_1(t) = 0, \quad u_{N+1}(t) = \frac{d\lambda}{dt}, \quad (30)$$

and initially $l_i(0) = 1$.

We note that if we knew the length of each cell $l_i(t)$, then (27) would give the corresponding osmotic potential. We therefore focus on the decoupled system (28)-(29).

3.4.3 Continuum limit

We assume that the length of the cells is small in comparison to the length of the endosperm, and take a continuum limit approximation of (28)-(29). We take s to be arc-length along the endosperm and let

$$l_i(t) \mapsto L(s, t) \text{ etc,} \quad \frac{dl_i}{dt} \mapsto \frac{DL}{Dt}, \quad (31)$$

where D/Dt is the convective derivative so that

$$u_{i+1} - u_i \sim L \frac{\partial u}{\partial s}. \quad (32)$$

From (28b) and (28c) we find

$$P_R = F \frac{\partial \theta}{\partial s}, \quad (33a)$$

$$F = 2T - 1, \quad (33b)$$

which gives the tension $T(s, t)$ in terms of the known angle of the centreline of the line of cells, $\theta(s, t)$, and the pressure exerted on the endosperm by the radicle, $P_R(s, t)$. From (28a), (29) and (32) we then obtain a system of two coupled PDEs

$$T(s, t) - Y = \mu(s, t) \frac{DL}{Dt}, \quad \frac{DL}{Dt} = L \frac{\partial u}{\partial s}, \quad (34)$$

subject to boundary conditions

$$u(0, t) = 0, \quad u(\lambda(t), t) = \frac{d\lambda}{dt}, \quad (35)$$

and initial condition $L(s, 0) = 1$.

3.4.4 Summary

In this section, we have developed a ‘Lockhart-style’ model of the endosperm to show how the individual cells stretch in response to the force from the radicle and the cell-wall weakening. Assuming the cells are small relative to the length of the micropylar region of the endosperm, we have taken a continuum limit, and it remains to solve the resulting coupled system of governing equations (34).

3.5 Viscous shell model

Alternatively, we may consider the endosperm to be a thin viscous sheet of fluid with fixed ends subjected to a pressure gradient across the sheet. Unlike the model derived in §3.4 this approach does not consider the individual characteristics of the cells; however, it can give information on the length scale of the endosperm. The imposed pressure gradient models the effect of the radicle on the endosperm; we note, however, that whilst this is not as physically realistic as modelling the radicle as a rigid or elastic body, it is significantly simpler than studying the full problem which would require incorporating the free boundary contact problem. The endosperm has a small aspect ratio, (*i.e.* it is much longer than it is wide), and so we may assume dependence only on the arclength, s , along the endosperm. Assuming that the sheet is flat in one direction, from [14] we have the nondimensionalised system

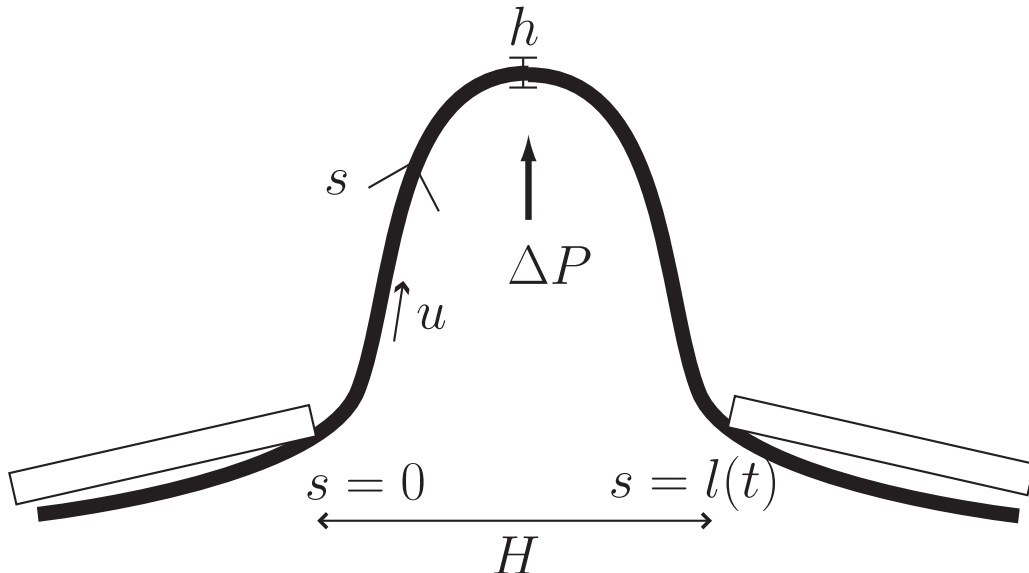


Figure 11: Diagrammatic representation of the viscous shell model (36)-(40).

$$\frac{\partial h}{\partial t} + \frac{\partial}{\partial s}(uh) = 0, \quad (36a)$$

$$\frac{\partial}{\partial s} \left(4\mu h \frac{\partial u}{\partial s} \right) = 0, \quad (36b)$$

$$4\mu h \frac{\partial u}{\partial s} \kappa + \Delta P = 0, \quad (36c)$$

where u is the velocity along the centreline of the sheet, h is the thickness of the sheet, θ is the angle the centreline makes with the horizontal, $\kappa = \partial\theta/\partial s$ is the curvature, ΔP is the imposed pressure gradient and μ is the viscosity. The endosperm degrades to allow growth and (eventually) rupture; therefore we take μ to be a function of both arclength and time.

We now consider boundary conditions. Whilst the ends of the sheet are fixed in Cartesian space, the total length of the sheet, λ , is a function of time, and therefore we have

$$u(0, t) = 0, \quad u(\lambda(t), t) = \frac{d\lambda}{dt}, \quad (37)$$

as boundary conditions on the velocity, along with

$$x(0, t) = 0, \quad y(0, t) = 0, \quad x(\lambda(t), t) = H, \quad y(\lambda(t), t) = 0, \quad (38)$$

where x, y are the Cartesian coordinates of the sheet which may be found via

$$\frac{\partial x}{\partial s} = \cos \theta, \quad \frac{\partial y}{\partial s} = \sin \theta, \quad (39)$$

and H is the horizontal distance between the two fixed ends of the sheet. Our final condition is

$$\int_0^{\lambda(t)} \cos \theta ds = H, \quad (40)$$

for the unknown length $\lambda(t)$.

We integrate (36b) to find

$$4\mu h \frac{\partial u}{\partial s} = T(t), \quad (41)$$

where T is the tension in the sheet. Upon substituting this into (36c), we learn that

$$T(t)\kappa + \Delta P = 0. \quad (42)$$

Therefore, if ΔP does not depend on space then neither does the curvature; taking viscosity to be a function of space and time does not alter this, although this will produce modified stresses which may allow the endosperm to rupture preferentially near the radicle tip. To see spatial variations in curvature, we could additionally solve the model with ΔP also varying in space. Alternatively, we may be looking on the wrong timescale for spatial variations in curvature to be captured.

There is some debate over what causes the modification of the viscosity of the endosperm. It could depend on time, on some externally produced hormone concentration, on the tension induced in the walls, on the local extension of a wall, or on any combination of these. This is an important question in germination, and the answer is not known. However, any of these may be incorporated into this model by modifying the expression for the viscosity to vary as appropriate. It remains to solve this model for an appropriate choice of μ , but the situation for constant μ and ΔP is considered in [14].

4 Conclusions

During seed germination both the radicle elongates and the endosperm weakens. The combination of these two processes cause the endosperm to stretch and eventually rupture so that

the radicle can protrude. These key aspects of seed germination have received relatively little attention from the mathematical modelling community. We now summarise our key results.

In §2, we considered a ‘Lockhart-style’ model of radicle elongation, modelling the radicle as a cylinder of fluid. Based on experimentally derived parameter estimates, we found regulation of the osmotic potential to be rapid, so the radicle is always fully turgid. The endosperm provides a force on the ends of the radicle which opposes radicle elongation. When the radicle reaches a prescribed length, the endosperm ruptures and so this opposing force is removed, leading to a rapid increase in the radicle’s length.

In §3, we modelled the endosperm, assuming that the radicle applies a constant normal force to the endosperm. We considered several options for the material properties: assuming the endosperm is elastic (§3.2–3), or viscous (§3.4–5). In §3.2, we first considered a simple spring model for the endosperm, and used experimental data to estimate a linear law for the weakening of the endosperm. We then showed how the spring model could be incorporated into a more complex computational model which consisted of a sheet of rigid cells joined by elastic springs (§3.3). In §3.4–5, we assumed the endosperm is viscous. In §3.4, we developed a ‘Lockhart-style’ model, considering the stretching of the individual cells in the endosperm. We then consider a tissue-scale model in §3.5, modelling the endosperm as a thin viscous sheet. In both these models, §3.4–5, solving the resulting system of governing equations is beyond the scope of this report.

Although many of the models considered have not been solved, our efforts illustrate how different aspects of seed germination are amenable to mathematical modelling. Determining which of the endosperm models is appropriate will require detailed comparison with experiments. We were provided with images of endosperm rupture which were taken at fifteen minutes intervals. Since rupture appears to be a rapid process, this did not provide sufficient information to determine the material properties. Taking images at shorter intervals close to the rupture time could provide detailed quantitative information about how the radicle lengthens and the endosperm stretches. We could then compare these data to our model results. Future modelling efforts will focus on coupling a model of radicle elongation to one of endosperm rupture.

References

- [1] R.M. Barroco, K. Van Poucke, J.H.W. Bergervoet, L. De Veylder, S.P.C. Groot, D. Inze, and G. Engler. The role of the cell cycle machinery in resumption of postembryonic development. *Plant Physiology*, 2005.
- [2] J.D. Bewley. Seed germination and dormancy. *The Plant Cell*, 9(7):1055, 1997.
- [3] E. Carrera, T. Holman, A. Medhurst, W. Peer, H. Schmuths, S. Footitt, F.L. Theodoulou, and M.J. Holdsworth. Gene expression profiling reveals defined functions of the ATP-binding cassette transporter COMATOSE late in Phase II of germination. *Plant Physiology*, 143(4):1669, 2007.
- [4] V. Lefebvre, H. North, A. Frey, B. Sotta, M. Seo, M. Okamoto, E. Nambara, and A. Marion-Poll. Functional analysis of Arabidopsis NCED6 and NCED9 genes indicates that ABA synthesized in the endosperm is involved in the induction of seed dormancy. *Plant J.*, 45(3):309–19, 2006.
- [5] P.P. Liu, N. Koizuka, T.M. Homrichhausen, J.R. Hewitt, R.C. Martin, and H. Nonogaki. Large-scale screening of Arabidopsis enhancer-trap lines for seed germination-associated genes. *The Plant Journal*, 41(6):936, 2005.
- [6] J.A. Lockhart. An analysis of irreversible plant cell elongation. *Journal of Theoretical Biology*, 1965.
- [7] N.H. Masubelele, W. Dewitte, M. Menges, S. Maughan, C. Collins, R. Huntley, J. Nieuwland, S. Scofield, and J.A.H. Murray. D-type cyclins activate division in the root apex to promote seed germination in Arabidopsis. *Proceedings of the National Academy of Sciences*, 102(43):15694–15699, 2005.

- [8] D.W. Meinke. Seed development in *Arabidopsis thaliana*. *Arabidopsis*, 27:253–295, 1994.
- [9] K. Muller, S. Tintelnot, and G. Leubner-Metzger. Endosperm-limited brassicaceae seed germination: abscisic acid inhibits embryo-induced endosperm weakening of *Lepidium sativum* (cress) and endosperm rupture of cress and *Arabidopsis thaliana*. *Plant and Cell Physiology*, 47(7):864–877, 2006.
- [10] S. Penfield, Y. Li, A.D. Gilday, S. Graham, and I.A. Graham. *Arabidopsis* ABA INSENSITIVE4 regulates lipid mobilization in the embryo and reveals repression of seed germination by the endosperm. *The Plant Cell Online*, 18(8):1887, 2006.
- [11] P. Schopfer and C. Plachy. Control of seed germination by abscisic acid: II. Effect on embryo water uptake in *Brassica napus* L. *Plant Physiology*, 76(1):155–160, 1984.
- [12] P. Schopfer and C. Plachy. Control of seed germination by abscisic acid III. Effect on embryo growth potential (minimum turgor pressure) and growth coefficient (cell wall extensibility) in *Brassica napus* L. *Plant Physiology*, 77(3):676–686, 1985.
- [13] S.N. Shabala and R.R. Lew. Turgor Regulation in Osmotically Stressed *Arabidopsis* Epidermal Root Cells. Direct Support for the Role of Inorganic Ion Uptake as Revealed by Concurrent Flux and Cell Turgor Measurements. *Plant Physiology*, 129(1):290, 2002.
- [14] B.W. Van De Fliert, P.D. Howell, and J.R. Ockenden. Pressure-driven flow of a thin viscous sheet. *J. Fluid Mech.*, 292:359–376, 2006.